NASA Technical Memorandum 88797

Quantitative Void Characterization in Structural Ceramics Using Scanning Laser Acoustic Microscopy

Don J. Roth and Edward R. Generazio
Lewis Research Center
Cleveland, Ohio

and

George Y. Baaklini
Cleveland State University
Cleveland, Ohio

Prepared for the
Basic Science, Electronics, and Glass Divisions Joint Meeting
sponsored by the American Ceramic Society
New Orleans, Louisiana, November 2–5, 1986

NASA

QUANTITATIVE VOID CHARACTERIZATION IN STRUCTURAL CERAMICS USING SCANNING LASER ACOUSTIC MICROSCOPY

Don J. Roth and Edward R. Generazio
National Aeronautics and Space Administration
Lewis Research Center
Cleveland, Ohio 44135

and

George Y. Baaklini
Cleveland State University
Cleveland, Ohio 44115

SUMMARY

The ability of scanning laser acoustic microscopy (SLAM) to characterize artificially seeded voids in sintered silicon nitride structural ceramic specimens was investigated. Using trigonometric relationships and Airy's diffraction theory, predictions of internal void depth and size were obtained from acoustic diffraction patterns produced by the voids. Agreement was observed between actual and predicted void depths. However, predicted void diameters were generally much greater than actual diameters. Precise diameter predictions are difficult to obtain due to measurement uncertainty and the limitations of 100 MHz SLAM applied to typical ceramic specimens.

INTRODUCTION

Structural ceramics such as silicon nitride (Si_3N_4) and silicon carbide (SiC) are candidate materials for hot section components in conventional and advanced heat engines (refs. 1 to 4). These materials have several advantages over presently-used metals including the ability to withstand higher operating temperatures (leading to increased fuel efficiency), greater resistance to corrosion and erosion, and an abundant, inexpensive, and nonstrategic supply of raw materials from which to form them (refs. 1 to 3). Structural ceramics exhibit wide variability in strength and low fracture toughness due to their brittle nature (refs. 3, 5 and 6). Failure is generally attributed to discrete flaws such as microcracks, voids, impurities, and oversized grains (refs. 7 to 11). The relationships between fracture strengths and flaw types, sizes, shapes, and locations are being actively investigated for structural ceramics (see fig. 1). Therefore, the ability to accurately characterize existing flaws in these materials by nondestructive evaluation (NDE) techniques has become extremely important.

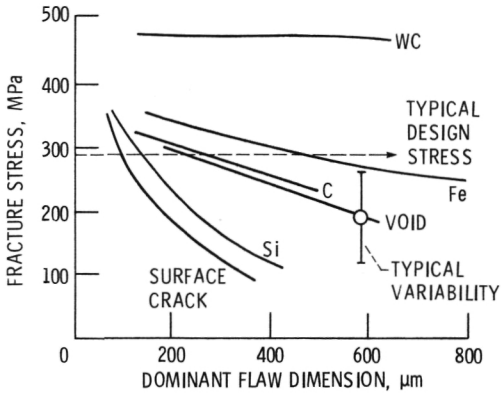

Figure 1. - Relations between fracture strength and flaw size for various types of flaws in silicon nitride. Reprinted by permission of the publisher from "ASPECTS OF THE RELIABILITY OF CERAMICS," pp. 63-80 IN DEFECT PROPERTIES AND PROCESSING OF HIGH-TECHNOLOGY NONMETALLIC MATERIALS, copyright 1984 by Elsevier Science Publishing Co., Inc.

Scanning laser acoustic microscopy (SLAM) is being evaluated as a potential NDE technique for characterizing flaw populations in structural ceramics (refs. 10, 12 to 14). Recent studies have investigated the reliability of SLAM for detecting voids in structural ceramic specimens (refs. 13 and 14) and the ability of SLAM to quantitatively characterize flaws in various materials (ref. 15). The former studies showed SLAM capable of reliably detecting voids over a wide size (30 to 430 μm) and depth (0 to 2 mm) range in sintered Si_3N_4. The latter study showed flaws embedded in homogeneous glass and plastic specimens to produce acoustic diffraction patterns that closely agree with those predicted theoretically; this indicated that SLAM may be useful for accurately characterizing (size, shape, and depth) flaws in ceramics. SLAM in the configuration studied in references 12 to 15 can generally inspect only sintered specimens having nearly flat and parallel surfaces. It is therefore presently useful for inspecting specimens such as modulus-of-rupture bars. Systems utilizing similar laser-acoustic technology may eventually be developed to inspect components having complex shapes.

This report describes a study in which the ability of 100 MHz SLAM to determine the size and depth of internal voids in sintered Si_3N_4 specimens was investigated. The specimens contained artificially implanted voids covering a wide size (20 to 430 μm) and depth (0 to 2 mm) range. Discrepancies between actual and predicted values are discussed.

PROCEDURE

Specimens

Sintered Si_3N_4 (SSN) specimens containing seeded internal voids were fabricated using the processing steps shown in figure 2 and described in detail in reference 16. Briefly, plastic microspheres of various sizes were embedded in green specimens and later burned out to create voids within sintered specimens. During formation of a specimen, a powder layer with the microspheres

exposed to the surface was photographed so that approximate planar positions of the resulting voids would be known for SLAM inspections.

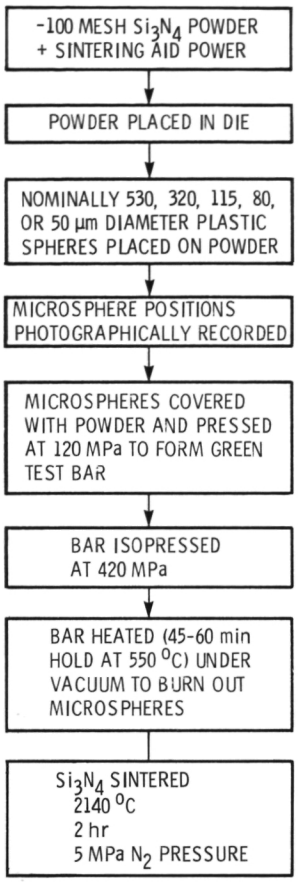

Figure 2. - Fabrication of the sintered silicon nitride test specimens with seeded internal voids.

Twelve seeded voids in seven SSN specimens were characterized according to size and depth using SLAM. The SSN specimens, similar in shape to modulus-of-rupture (MOR) test bars, are described in detail in Table I. They were approximately 100 percent of theoretical density and the average grain size was approximately 0.5 to 1.5 μm. The specimens were alternately ground (to remove material) and inspected with SLAM so that the seeded voids were positioned closer to the ground surface after each grinding step. In this manner, void sizes and depths could be predicted experimentally for various void positions beneath the surface. The surface grinding procedure was performed by hand using a 15, 30, or 45 μm (depending on the amount of material to be removed) diamond disc attached to a rotating metallographic polishing wheel. As a result of this procedure, the maximum peak-to-valley surface roughness of the ground surface varied from 0.5 to 3.5 μm depending on the specimen and inspection but was always relatively ordered (unidirectional). The opposite surface was left in the as-fired (unground) condition. Its maximum peak-to-valley surface roughness varied from 3.0 to 7.5 μm depending on the specimen but was randomly oriented for all specimens. The specimen thickness, measured after each grinding step using a digital micrometer accurate to 1 μm, varied from 2 to 4 mm.

TABLE I. - CHARACTERIZATION OF SPECIMENS

TEST BAR MATERIAL	NUMBER OF TEST BARS USED	LENGTH X WIDTH, (mm)	THICKNESS, (mm)	DENSITY		POROSITY DISTRIBUTION	AVERAGE GRAIN SIZE, (μm)	PEAK-TO-VALLEY ROUGHNESS, (μm), OF -		SEEDED INTERNAL VOIDS[g]		
				(g/cc)	% THEORETICAL			GROUND SURFACE	AS-FIRED SURFACE	TOTAL NUMBER	DIAMETER, (μm)	DEPTH BELOW SPECIMEN SURFACE (mm)
SINTERED Si_3N_4 (SSN)	7	30x6	2-4	3.230	~100	LESS AT EDGE THAN AT CENTER	0.5-1.5[c]	RELATIVELY ORDERED 0.5-3.5[e]	RANDOMLY ORIENTED 3.0-7.5[e]	12	20-430	0-2

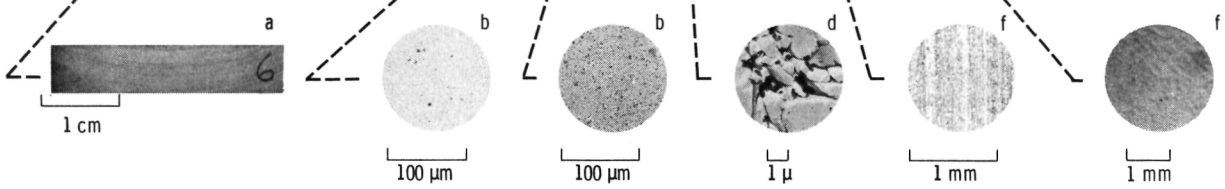

[a]OPTICAL PHOTOGRAPH (GROUND SURFACE SHOWN).
[b]OPTICAL MICROGRAPH OF METALLOGRAPHICALLY POLISHED SECTION (BLACK SPOTS INDICATE POROSITY).
[c]AVERAGE GRAIN SIZES OBTAINED USING THE HEYN INTERCEPT (MEAN FREE PATH) METHOD GIVEN IN ASTM E112-81.
[d]TRANSMISSION ELECTRON MICROGRAPH OF REPLICA OF METALLOGRAPHICALLY POLISHED AND ETCHED SECTION
[e]SURFACE PROFILE (USING A 12.5 μm DIAMETER DIAMOND STYLUS) (PERPENDICULAR TO GRINDING MARKS FOR SPECIMEN WITH GROUND SURFACE).
[f]OPTICAL MICROGRAPH.
[g]CHARACTERIZED AFTER SINTERING SPECIMEN AND EXPOSING VOIDS TO SURFACE.

The seeded internal voids were ultimately exposed to the surface by grinding. At this point, the void dimensions were measured optically and the void depths at the various SLAM inspections were determined (see fig. 3).

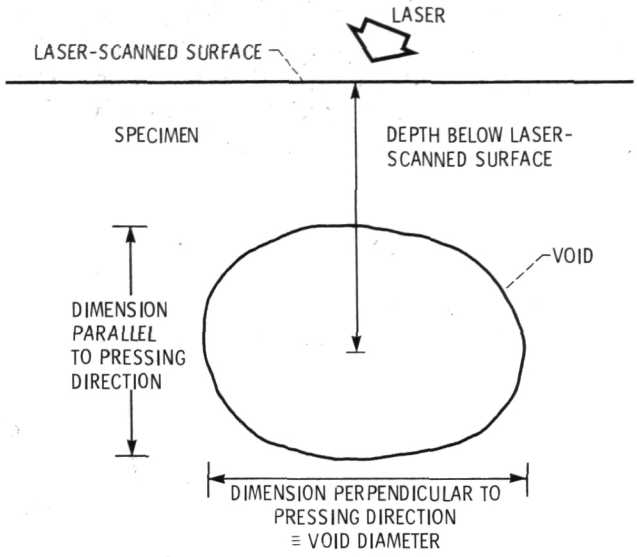

(a) Illustration showing definitions of void diameter and depth of void below the laser-scanned surface. Voids had an ellipsoidal geometry.

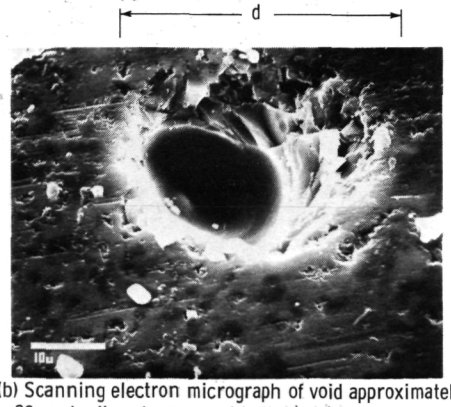

(b) Scanning electron micrograph of void approximately 30 μm in diameter exposed to the surface.

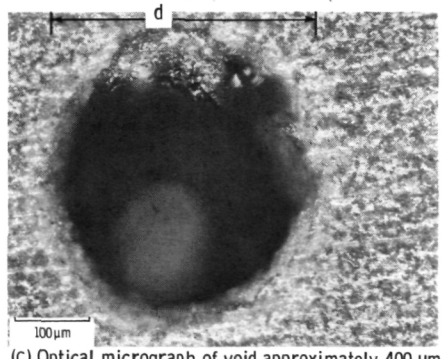

(c) Optical micrograph of void approximately 400 μm in diameter exposed to the surface.

Figure 3. - Seeded voids in sintered silicon nitride specimens.

The voids were ellipsoidal (ref. 16) with the dimension of the void perpendicular to the specimen pressing direction always larger than the dimension parallel to the pressing direction. The larger dimension was taken to be the void diameter. Void depth at a particular SLAM inspection was determined by subtracting the specimen thickness at which the void was ground open to the surface (to approximately the center of the void) from the thickness associated with the particular inspection. The voids ranged from 20 to 430 μm in diameter and were positioned at depths ranging up to 2 mm below the surface. The estimated uncertainties in the actual dimension and depth measurements were approximately +10 and ±5 percent, respectively.

Scanning Laser Acoustic Microscopy

The SLAM apparatus used for inspection of the ceramic test bars is shown in figure 4 and described in detail in references 12, 13, and 17.

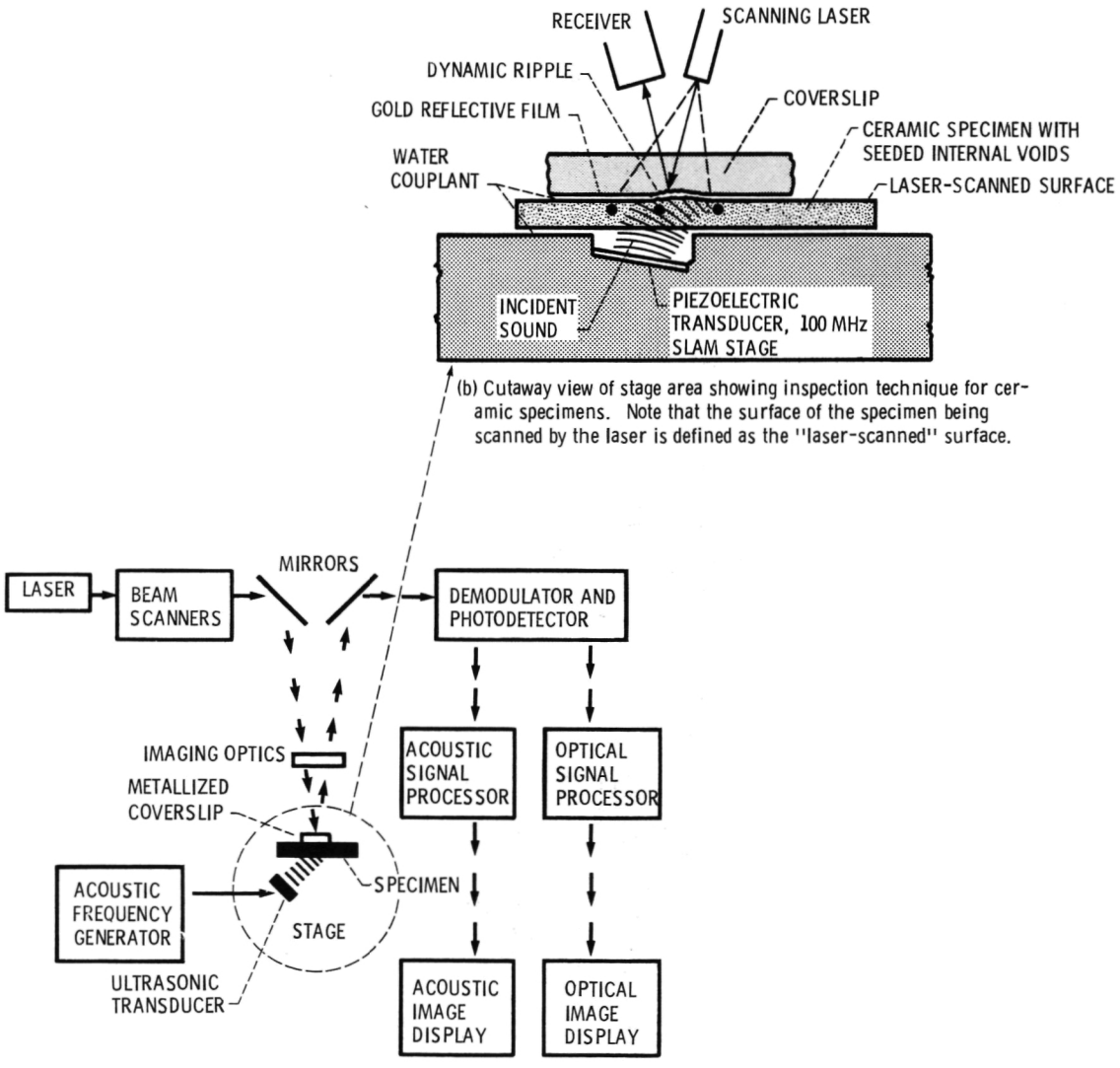

(b) Cutaway view of stage area showing inspection technique for ceramic specimens. Note that the surface of the specimen being scanned by the laser is defined as the "laser-scanned" surface.

(a) Schematic diagram of scanning laser acoustic microscope.

Figure 4. - Scanning laser acoustic microscopy.

Briefly, continuous 100 MHz ultrasonic waves traveling through the specimen produce microdistortions on the specimen surface opposite the incident sound source (surface nearest the laser). In this investigation, this surface was diamond ground (as described previously) and is herein defined as the laser-scanned surface. The distortion pattern, determined by the microstructural, bulk, and surface features of the material, is transmitted via water coupling to the reflective coating of a plastic coverslip placed on the specimen. A laser beam constantly raster scans an approximately 2.0 mm by 1.8 mm area of the coverslip. The laser beam, angularly modulated by the distortion pattern, is reflected to a photodetecter and converted to an electronic signal. In this manner, an "acoustic" image of the specimen, including surface and internal flaws such as voids, inclusions, and cracks, is obtained and displayed on a video monitor in real-time at approximately 100x magnification.

The acoustic image of an internal flaw often consists of a diffraction pattern as shown in figure 5 rather than a facsimile image of the flaw (refs. 15, 17 and 18). In this case, it is especially difficult to characterize the flaw. However, techniques have been investigated from which it is theoretically possible to predict flaw shape, size and depth using acoustic diffraction patterns (refs. 15, 17 to 19). The central maximum, first minimum, and uncertainty associated with the first minimum ($2a_1$, $2a_2$) are highlighted in figure 5 for the diffraction pattern of a naturally occurring subsurface void in glass.

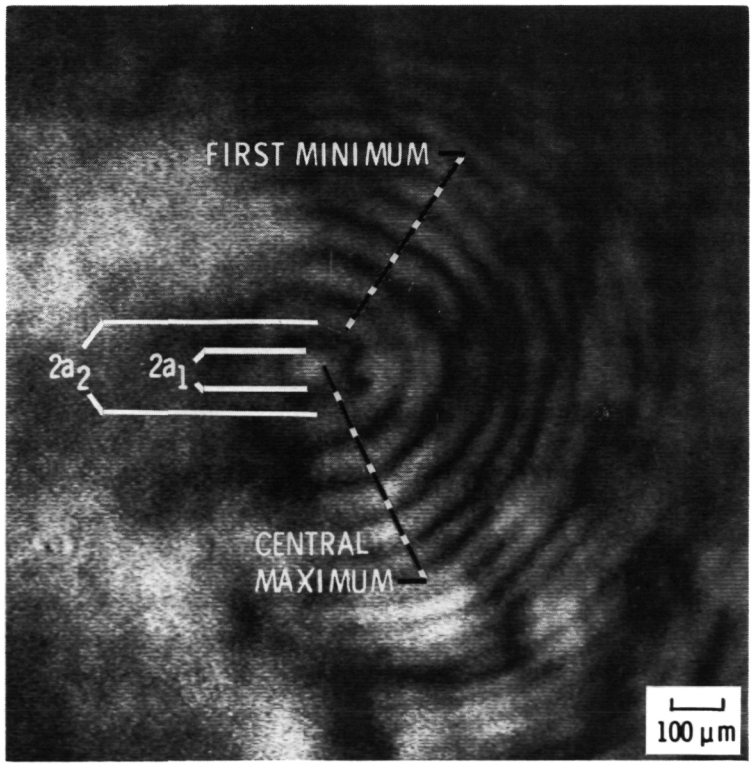

Figure 5. - Acoustic image of naturally occurring subsurface spherical void in glass.

Void Depth Prediction

A stereoscopic method using the acoustic images obtained with SLAM has previously been used to determine the depth of internal flaws in various materials (ref. 17) and is shown in figure 6. With this method, void depth, x, is given by

$$x = \frac{\ell}{2 \tan \beta_c} \tag{1}$$

where

$$\ell = \left| P_{180} - P_0 \right| \tag{2}$$

P_0 is the initial position of the acoustic diffraction pattern of the void and P_{180} is the position of the diffraction pattern of the void after rotating the specimen 180° about P_0. In this investigation, ℓ was determined by

$$\ell = \frac{\ell_1 + \ell_2}{2} \tag{3}$$

as shown in figure 6.

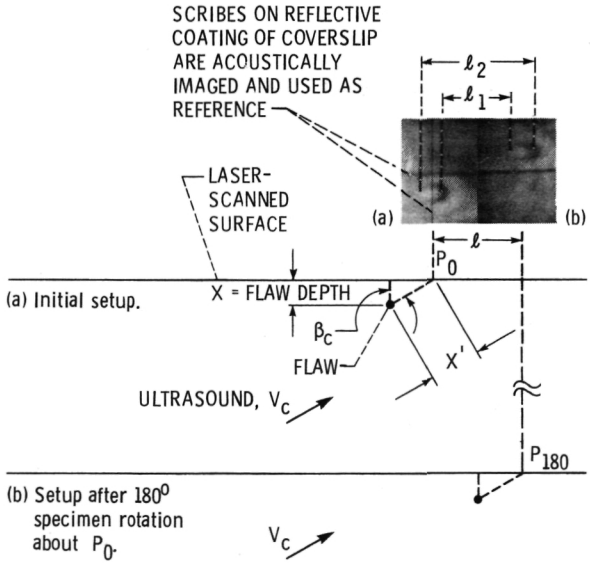

Figure 6. - Schematic diagrams showing principles of stereoscopic method used to determine depth of flaw beneath sample surface. P_0 and P_{180} are positions of flaw images ($\ell = P_{180} - P_0$).

β_c is the angular direction of the ultrasound in the ceramic and can be determined using Snell's law (ref. 20) or the shadow method described in references 15 and 17. For purposes of comparison, both methods were used to determine β_c in the SSN specimens. Void depth and diameter predictions were then obtained using both values of β_c. Using Snell's law

$$\beta_c = \sin^{-1}\left(\sin \beta_w \cdot \frac{V_c}{V_w}\right) \tag{4}$$

where β_w is the angular direction of ultrasound in the water couplant, and V_w and V_c are the velocity of ultrasound in the water and ceramic, respectively. In this study, $\beta_w = 10°$, $V_w = 0.149 \times 10^6$ cm/sec, and V_c for each SSN specimen was measured using a cross correlation method (ref. 21). Both longitudinal and shear velocities were measured. According to equation (4), however, only the shear wave component is utilized in the SSN with $\beta_w = 10°$ (i.e., 10° exceeds the critical angle for the water-SSN configuration if longitudinal velocities are substituted for V_c). Substituting equation (4) into equation (1), the predicted void depth using β_c obtained with Snell's law is

$$x = \frac{\ell}{2 \cdot \tan\left(\sin^{-1}\left[\sin \beta_w \cdot \frac{V_c}{V_w}\right]\right)} \tag{5}$$

The configuration for the shadow method is shown in figure 7(a). A rectangular groove or channel cut into the specimen surface as shown in figure 7(b) prevents ultrasound from reaching a limited area of the surface. This area, which shows up as an extremely dark (low-sound-intensity) region compared to adjacent areas in the acoustic image as shown in figure 7(c), is defined as the shadow region. Using the shadow method

$$\beta_c = \tan^{-1}\left(\frac{L}{H}\right) \tag{6}$$

where L is the length of the shadow region and H is the height of the channel. In this study, channels approximately 1 mm high were cut into the specimens (see fig. 7(b)) with a circular diamond blade. The channel corners were rounded due to the shape of the blade and H was determined by

$$H = \frac{H_1 + H_2}{2} \tag{7}$$

as shown in figure 7(b). The shadow region was not precisely defined and L was determined by

$$L = \frac{L_1 + L_2}{2} \tag{8}$$

as shown in figure 7(c). Substituting equation (6) into equation (1), the predicted void depth using β_c obtained with the shadow method is

$$x = \frac{\ell \cdot H}{2 \cdot L} \tag{9}$$

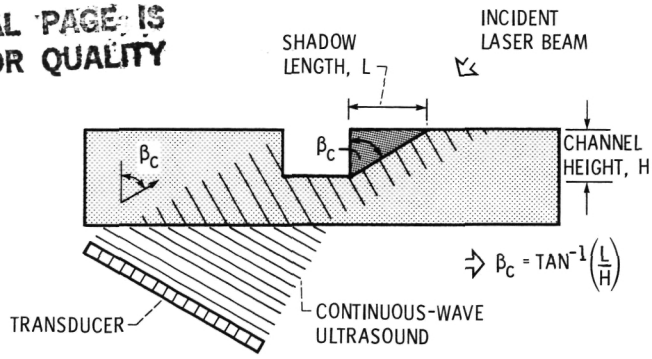

(a) Schematic diagram showing shadow region produced when ultrasound encounters rectangular channel in laser-scanned surface.

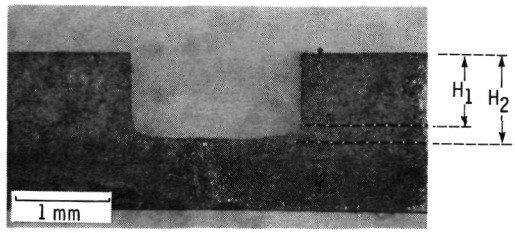

(b) Optical micrograph of channel in sintered silicon nitride specimen.

Figure 7. - Shadow method for determining ultrasound direction, β_c.

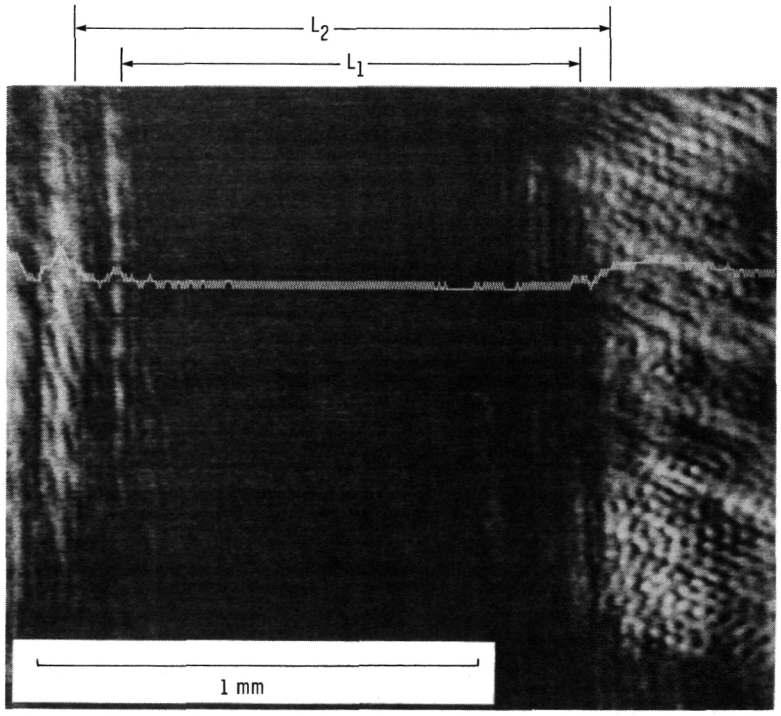

(c) Acoustic images taken near channel 7 (b) showing shadow region. Continuous white curve shows image intensity as a function of horizontal position.

Figure 7. - Concluded.

Void Size Prediction

Fraunhofer diffraction conditions are given by reference 19 as

$$x' > \frac{d^2}{4\lambda_c} \tag{10}$$

where x' is the distance between a flaw of circular cross section and the image plane, d is the flaw diameter, and λ_c is the wavelength of ultrasound in the ceramic. Assuming Fraunhofer diffraction, the flaw diameter can be determined according to the Airy relation (refs. 19, 20 and 22)

$$d = \frac{1.22\lambda_c}{\sin \theta} \tag{11}$$

where θ is the angle at which the first minimum of the diffraction pattern occurs. λ_c is determined by

$$\lambda_c = \frac{V_c}{f} \tag{12}$$

where f is the frequency of ultrasound (100 MHz). As shown in figure 8, θ can be determined from

$$\theta = \tan^{-1}\left(\frac{a}{x'}\right) \tag{13}$$

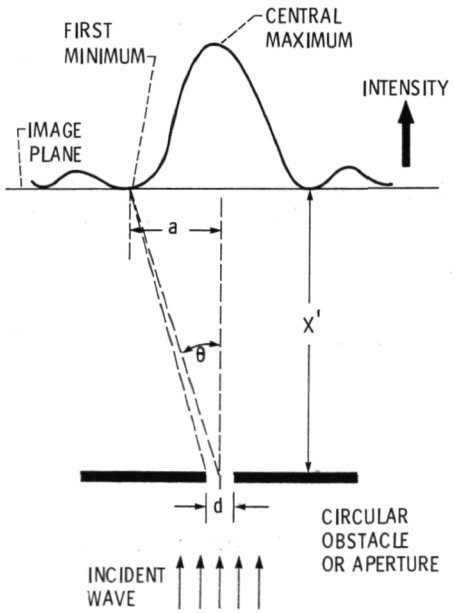

Figure 8. - Schematic of diffraction pattern produced by circular aperture or obstacle assuming Fraunhofer diffraction conditions.

where a is the distance between the central maximum and the first minimum. The maximums and minimums were not precisely defined and 2a (twice the distance between the central maximum and the first minimum) was determined by

$$2a = \frac{2a_1 + 2a_2}{2} \tag{14}$$

as shown in figure 5.

For our experiment, x' is the distance between the image plane (laser-scanned surface) and the flaw relative to the ultrasonic direction as shown in figure 6.

x' is given by

$$x' = \frac{x}{\cos \beta_c} \tag{15}$$

Combining equations (4), (5), (11), (12), (13), and (15), the predicted void diameter using β_c obtained with Snell's law is

$$d = \frac{1.22V_c}{f} \cdot \left[\csc \left\{ \tan^{-1} \left(\frac{2a}{\ell} \cdot \tan \left[\sin^{-1} \left\{ \sin \beta_w \cdot \frac{V_c}{V_w} \right\} \right] \right. \right. \right. \cdot \left. \left. \left. \cos \left(\sin^{-1} \left\{ \sin \beta_w \cdot \frac{V_c}{V_w} \right\} \right) \right) \right\} \right] \tag{16}$$

Combining equations (6), (9), (11), (12), (13), and (15), the predicted void diameter using β_c obtained with the shadow method is

$$d = \frac{1.22V_c}{f} \cdot \left[\csc \left\{ \tan^{-1} \left(\frac{2a \cdot L \cdot \cos \left[\tan^{-1} \left(\frac{L}{H} \right) \right]}{\ell \cdot H} \right) \right\} \right] \tag{17}$$

Deviation and Uncertainty

The percent deviation in the predicted void depth was calculated from

$$D_x = \left(\frac{x_a - x_p}{x_a} \right) 100\% \tag{18}$$

where x_a is the actual depth and x_p is the predicted depth. The percent deviation in the predicted void diameter was calculated from:

$$D_d = \left(\frac{d_a - d_p}{d_a} \right) 100\% \tag{19}$$

where d_a is the actual diameter and d_p is the predicted diameter.

Several measurements were required for void depth (ℓ, H, and L) and diameter (2a, ℓ, H, and L) predictions using equations (9) and (17), respectively. As shown in figures 5, 6, 7(b) and (c), these measurements had uncertainty associated with them. The uncertainty in the predicted void diameter due to the uncertainty in the required measurements was obtained using equation (17) and the variance relation (ref. 23) to give

$$\sigma_d^2 = \left(\frac{\partial d}{\partial (2a)} \right)^2 \cdot \Delta(2a)^2 + \left(\frac{\partial d}{\partial \ell} \right)^2 \cdot (\Delta \ell)^2 + \left(\frac{\partial d}{\partial L} \right)^2 \cdot (\Delta L)^2 + \left(\frac{\partial d}{\partial H} \right)^2 \cdot (\Delta H)^2 \tag{20}$$

with percent uncertainty given by

$$U_d = \left| \frac{\sigma_d}{d_a} \right| 100\% \tag{21}$$

where

$$\Delta 2a = 2a_2 - 2a_1 \tag{22}$$

$$\Delta \ell = \ell_2 - \ell_1 \tag{23}$$

$$\Delta L = L_2 - L_1 \tag{24}$$

and

$$\Delta H = H_2 - H_1 \tag{25}$$

as shown in figures 5, 6, 7(c), and (b), respectively.

RESULTS AND DISCUSSION

Void depth and diameter predictions using SLAM are given for four representative voids from four different specimens in tables II and III, respectively. The four voids, 403, 252, 139, and 30 μm in diameter, were inspected at depths ranging from approximately 250 to 1900 μm, 100 to 1500 μm, 100 to 900 μm, and 50 to 125 μm, respectively. The largest depth given for each void represents the depth below the laser-scanned surface at which the void was first detected (depth at which the first minimum of the acoustic diffraction pattern was initially observed) (ref. 14). The smallest depth represents the depth at which the acoustic diffraction pattern became slightly disordered and the distance 2a was difficult to determine.

TABLE II. - PREDICTED VOID DEPTHS USING SLAM

Actual void diameter (μm)	Actual void depth (μm)	Shadow method			Snell's law		
		β_{ssn} (deg)	Predicted depth (μm)	Percent deviation from actual depth	β_{ssn} (deg)	Predicted depth (μm)	Percent deviation from actual depth
403	1897	47.6	1917	-1.1	45.3	2078	-9.5
	1517		1447	+4.6		1568	-3.4
	1176		1196	-1.7		1296	-10.2
	859		817	+4.9		886	-3.1
	554		580	-4.7		628	-13.4
	361		393	-8.9		425	-17.7
	263		320	-21.7		346	-31.6
252	1473	45.9	1519	-3.1	44.9	1568	-6.4
	922		942	-2.2		972	-5.4
	568		616	-8.5		636	-12.0
	253		242	+4.3		250	+1.2
	141		73	+48.2		75	+46.8
139	870	51.8	731	+16.0	45.6	911	-4.7
	686		625	+8.9		738	-7.6
	507		507	0.0		632	-24.7
	307		295	+3.9		367	-19.5
	197		153	+22.3		191	+3.0
	148		108	+27.0		135	+8.8
30	116	42.9	188	-62.1	44.5	180	-55.2
	89		81	+9.0		76	+14.6
	79		54	+31.6		51	+35.4
	67		65	+3.0		61	+9.0
	52		54	-3.8		51	+1.9

TABLE III. - PREDICTED VOID DIAMETERS USING SLAM

Actual void diameter (μm)	Actual void depth (μm)	Shadow method			Snell's law			Percent uncertainty in predicted diameter computer from Eq. (21)
		β_{ssn} (deg)	Predicted diameter (μm)	Percent deviation from actual diameter	β_{ssn} (deg)	Predicted diameter (μm)	Percent deviation from actual diameter	
403	1897	47.6	1113	-176.2	45.3	1156	-186.8	148
	1517		1035	-156.8		1075	-166.7	129
	1176		1080	-168.0		1122	-178.4	160
	859		894	-121.8		928	-130.3	93
	554		901	-123.6		936	-132.3	156
	361		861	-113.6		894	-121.8	142
	263		792	-96.5		822	-104.0	147
252	1473	45.9	1132	-349.2	44.9	1150	-356.3	383
	922		751	-198.0		763	-202.8	182
	568		790	-213.5		802	-218.3	289
	253		419	-66.3		425	-68.7	143
	141		228	+9.5		232	-7.9	112
139	870	51.8	624	-348.9	45.6	686	-393.5	246
	686		558	-301.4		613	-341.0	250
	507		467	-236.0		513	-269.1	119
	307		504	-262.6		554	-298.6	226
	197		571	-310.8		628	-351.8	302
	148		495	-256.1		543	-290.6	291
30	116	42.9	211	-603.3	44.5	206	-586.7	484
	89		144	-380.0		141	-370.0	518
	79		135	-350.0		132	-340.0	311
	67		148	-393.3		144	-380.0	442
	52		157	-423.3		154	-413.3	387

Tables II and III list 23 predicted values determined using β_c obtained from both the shadow method and Snell's law. Deviations from actual values are also given. Additionally, the percent uncertainty in the predicted void diameter determined from equation (21) is given in the last column of table III. As shown in table II for each specimen, the values of β_c obtained with the shadow method and Snell's law were similar with the maximum difference (approximately 13 percent) occurring for the specimen containing the 139 μm void. It is therefore likely that both methods are valid for determining ultrasonic direction (at 100 MHz) in fully dense structural ceramic specimens having surface roughnesses and microstructures similar to the specimens used in this study.

Void Depth Prediction

Table IV summarizes the agreement seen between predicted and actual void depths.

TABLE IV. - AGREEMENT BETWEEN ACTUAL AND PREDICTED VOID DEPTHS

Percent deviation between actual and predicted void depth	Number (out of 23) of predicted depths with less than corresponding percent deviation	
	Shadow method	Snell's law
5	11	5
10	16	12
20	17	18
30	20	19
40	21	21
50	22	22
60	22	23
70	23	23

Using the shadow method to determine β_c, the 23 predicted void depths deviated less than 70 percent from actual depths and 17 were within 20 percent of actual depths. Using Snell's law to determine β_c, the 23 predicted void depths deviated less than 60 percent from actual depths and 18 were within 20 percent of actual values. Obvious trends were not observed in the deviations associated with predicted void depths as shown in Table II. The smallest and largest deviations occurred randomly throughout the respective depth ranges investigated for each of the four voids. Uncertainty present in the measurements of ℓ, L and H (see eqs. (23), (24), and (25) and figs. 6, 7(c), and (b), respectively) used to determine void depth (see eq. (9)) may account for the deviations.

Void Diameter Prediction

Predicted void diameters determined using β_c obtained from both the shadow method and Snell's law deviated more than 100 percent from actual values in most cases as shown in the percent deviation columns of table III. The deviations were as large as 500 to 600 percent in some cases with most predicted diameters greater than actual diameters. The percent uncertainties in the predicted void diameters determined by substituting the appropriate experimental values into equation (21) are of the same order of magnitude as the corresponding percent deviations. Uncertainties in the measurement of 2a (see fig. 5) and ℓ (see fig. 6) were dominant in determining the uncertainty in the predicted void diameter. Precise measurements of these quantities were not possible making precise void diameter predictions difficult to obtain.

Figures 9(a) and (b) show theoretically expected percent uncertainties in predicted void diameters as functions of true void diameter and depth. For these figures, percent uncertainty was calculated from equation (21) using varying values of void depth (0 to 1 mm) and void diameter (75 to 500 μm), and fixed values of f, β_c, V_c, H, ΔH, L, ΔL, $\Delta \ell$, and $\Delta 2a$. (The fixed values were those experimentally obtained for the specimen containing the 403 μm void.) Figures 9(a) and (b) show that percent uncertainty in predicted

void diameter increases with increasing void diameter and decreasing void depth (as void approaches laser-scanned surface). In other words, larger uncertainties in predicted void diameter are expected for larger voids positioned closer to the laser-scanned surface while smaller uncertainties are expected for smaller voids positioned further from the laser-scanned surface. As examples, for a 500 μm void located 50 μm below the laser-scanned surface and a 75 μm void located 1000 μm below the laser-scanned surface, percent uncertainty is approximately 250 and 10 percent, respectively.

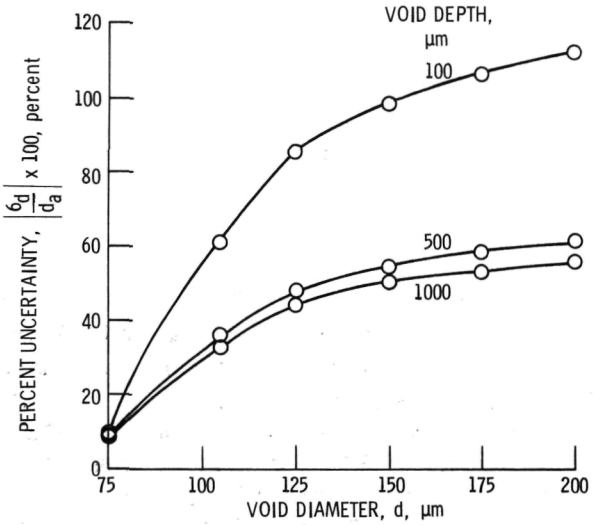

(a) Percent uncertainty versus void diameter for various void depths.

Figure 9. - Percent uncertainty in predicted void diameter determined from equation (21) as a function of void diameter and depth.

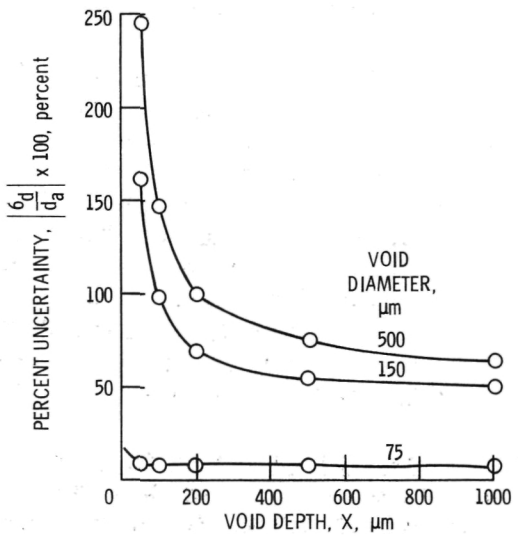

(b) Percent uncertainty versus void depth for various void diameters.

Figure 9. - Concluded.

Conditions may have been present which further explain the discrepancies that existed between predicted and actual void diameters. Figure 10 shows a plot of void depths and diameters defining conditions for Fresnel ($x' < d^2/4\lambda_c$) and Fraunhofer ($x' > d^2/4\lambda_c$) diffraction for voids in SSN. Airy's relation (eq. (11)) is most valid for conditions defined approximately by $x' >> d^2/\lambda_c$ (refs. 19 and 22), i.e., in a region defined in figure 10 as the extreme Fraunhofer region ($x' > 100(d^2/4\lambda_c)$). It is expected that for voids not satisfying extreme Fraunhofer diffraction conditions, phase cancellation at the minimums (see figs. 5 and 8) is incomplete resulting in displaced minimums (ref. 15) and therefore less accurate void diameter predictions using the Airy relation. The range of void depths and diameters that produced discernible diffraction patterns in this study is shown in figure 10 (experimental data region). As shown, most diffraction patterns were observed in the Fraunhofer region, but not in the extreme Fraunhofer region. In fact, extreme Fraunhofer conditions are difficult to approach with the 100 MHz SLAM configuration applied to typical ceramic specimens. For example, a 100 μm void must be approximately 3 mm below the laser-scanned surface in SSN to approach extreme Fraunhofer diffraction conditions. For voids of this diameter and depth in SSN, diffraction patterns produced by the voids are not able to be observed in the acoustic image using the SLAM configuration of figure 4. For $d = 100$ μm and $x = 3$ mm, $2a$ (determined from eq. (17)) (see fig. 5) is approximately 10 mm which is much greater than the distance scanned by the SLAM laser (approximately 2 mm). Therefore the diffraction pattern would not be seen on the video monitor. Note that even if diffraction patterns could be observed in the extreme Fraunhofer region, large uncertainties in the measurements of $2a$ and ℓ would still be present as previously described.

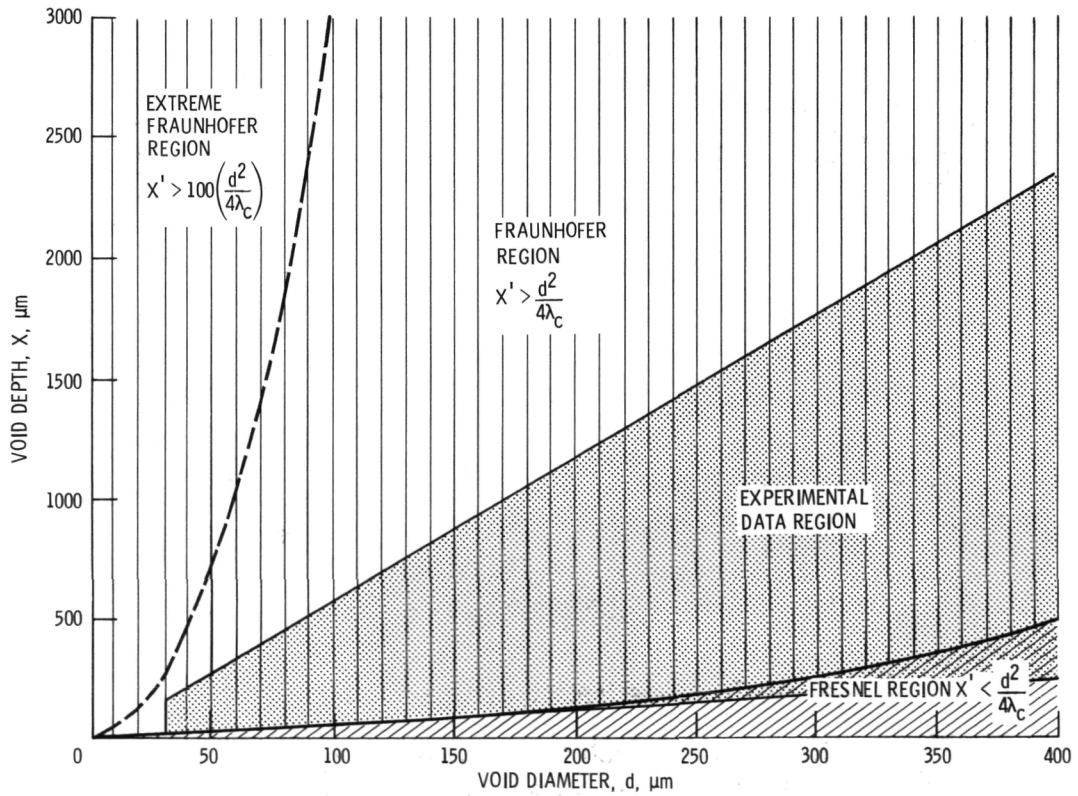

Figure 10. - Void depths and diameters defining conditions for Fresnel and Fraunhofer diffraction for voids in sintered silicon nitride.

Other conditions may have caused discrepancies to occur between predicted and actual void diameters. In a study described in reference 16, sintering aid material was present in areas surrounding seeded voids in SSN specimens manufactured similarly to those used in this investigation (see fig. 11).

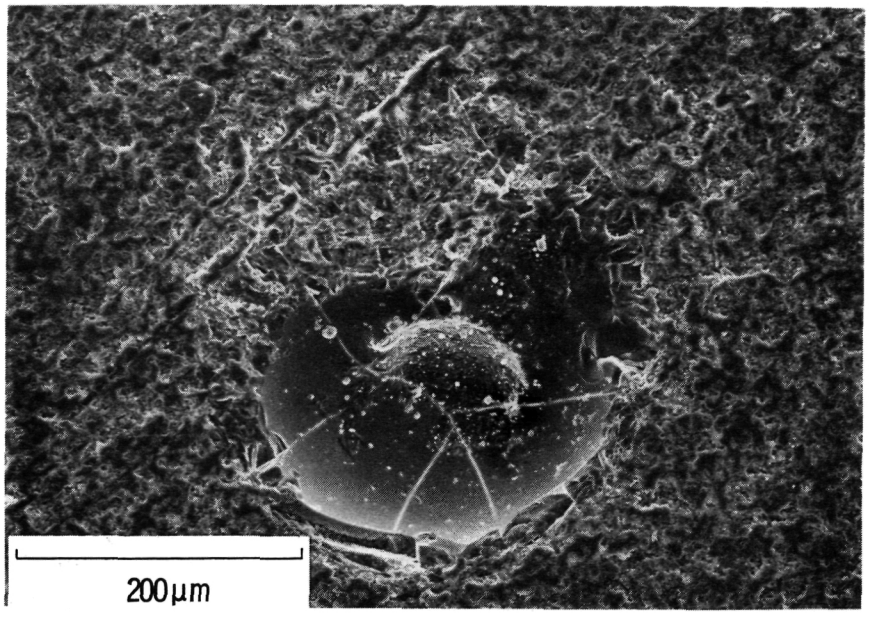

(a) As exposed to surface.

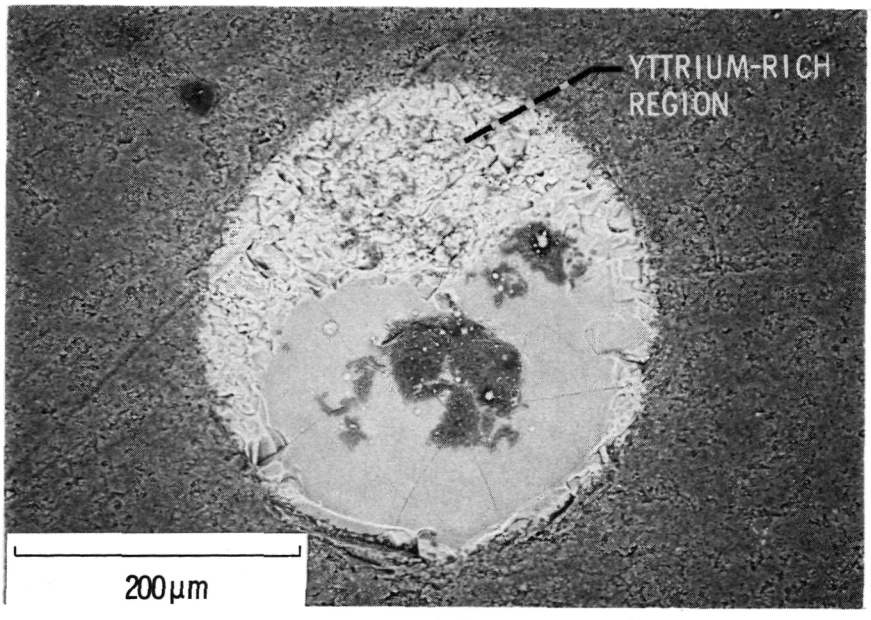

(b) Backscattered electron image of same region.

Figure 11. - Scanning electron micrographs of internal voids in sintered silicon nitride. Backscattered electron image (b) highlights yttrium-rich region.

Scatterers associated with those seeded voids were expected to be larger than the optically measured voids. Although it was not determined, areas of sintering aid material may also have been present surrounding the seeded voids in the SSN specimens investigated in this study.

Two conditions existed that did not fulfill theoretical requirements necessary for the successful application of the Airy relation as shown in figure 8. First, the voids (scatterers) did not have a circular cross section (see figs. 3 and 11). Second the diffraction patterns produced by the voids were observed on an image plane not perpendicular to the direction of sound propagation (see fig. 6).

CONCLUSION

The ability of scanning laser acoustic microscopy (SLAM) to characterize artificially seeded voids in sintered silicon nitride structural ceramic specimens according to size and depth was investigated. Using trigonometric relationships and Airy's diffraction theory, predictions of void depth and diameter were obtained from acoustic diffraction patterns produced by the voids. Agreement was observed between predicted and actual void depths. For 23 predicted depths, 17 deviated less than 20 percent from actual depths. Predicted void diameters were generally much larger than actual void diameters. Deviations were as large as 500 to 600 percent in some cases. It was shown that uncertainties in the measurements used to obtain predicted void diameter accounted for the deviations between predicted and actual diameters. Also, diffraction patterns were observed in regions for which the Airy relation is of questionable validity. Summarizing, precise diameter predictions are difficult to obtain due to measurement uncertainty and the limitations of 100 MHz SLAM applied to typical ceramic specimens.

REFERENCES

1. A.P.S. Teotia, and L.R. Johnson, "Structural Ceramics in Transportation: Fuel Implications and Economic Aspects," CONF-850115-4, Dept. of Energy, 1985.

2. R.N. Katz, "Ceramics for Vehicular Engines: State-of-the-Art," pp. 449-467 in Energy and Ceramics, Edited by P. Vicenzini, Elsevier, New York, 1980.

3. E.M. Lenoe, "Recent Accomplishments and Research Needs in Structural Ceramics," pp. 3-18 in Ceramics for High-Performance Applications III: Reliability, Edited by E.M. Lenoe, R.N. Katz and J.J. Burke, Plenum Press, New York, 1983.

4. S. Bortz, "Reliability of Ceramics for Heat Engine Applications," pp. 445-473 in Ceramics for High-Performance Applications III: Reliability, Edited by E.M. Lenoe, R.N. Katz and J.J. Burke, Plenum Press, New York, 1983.

5. J.L. Shannon, Jr., R.T. Bubsey, D. Munz, W.S. Pierce, "Fracture Toughness of Brittle Materials Determined with Chevron Notch Specimens," pp. 1127-1144 in Advances in Ceramic Research (Fracture '81). Edited by D. Francois, Pergamon, New York, 1981.

6. J.A. Salem, J.L. Shannon Jr., "Fracture Toughness of Si_3N_4 Measured with Short Bar Chevron-Notched Specimens," NASA TM-87153, 1985.

7. A.G. Evans, "Aspects of the Reliability of Ceramics," pp. 63-80 in Defect Properties and Processing of High-Technology Nonmetallic Materials, Edited by J.H. Crawford Jr., Y. Chen, and W.A. Sibley, North Holland, New York, 1984.

8. A.G. Evans, G.S. Kino, B.T. Khuri-Yakub, and B.R. Tittman, "Failure Prediction in Structural Ceramics," Mater. Eval., 35, [4] 85-96 (1977).

9. A.G. Evans, "Structural Reliability: A Processing-Dependent Phenomenon," J. Am. Ceram. Soc., 65, [3] 127-137 (1982).

10. P.W. Heitman and P.K. Khandelwal, "Development and Characterization of Ceramic Turbine Components," pp. 645-664 in Ceramics for High-Performance Applications III: Reliability, Edited by E.M. Lenoe, R.N. Katz and J.J. Burke, Plenum Press, New York, 1983.

11. W.A. Sanders, G.Y. Baaklini, "Correlation of Processing and Sintering Variables with the Strength and Radiography of Silicon Nitride," NASA TM-87251, 1986.

12. D.S. Kupperman, L. Pahis, D. Yuhas, and T.E. McGraw, "Acoustic Microscopy Techniques for Structural Ceramics," Am. Ceram. Soc. Bull., 59 [8] 814-816, 839-841 (1980).

13. D.J. Roth, S.J. Klima, J.D. Kiser, and G.Y. Baaklini, "Reliability of Void Detection in Structural Ceramics by Use of Scanning Laser Acoustic Microscopy," Mater. Eval., May 1986, 44, [6] 762-769,761 (1986).

14. D.J. Roth and G.Y. Baaklini, "Reliability of Scanning Laser Acoustic Microscopy for Detecting Internal Voids in Structural Ceramics," Adv. Ceram. Mater., 1 [3] (1986), July, pp. 252-258. Also NASA TM-87222.

15. E.R. Generazio and D.J. Roth, "Quantitative Flaw Characterization with Scanning Laser Acoustic Microscopy," Mater. Eval., 44 [7] 863-870 June (1986).

16. G.Y. Baaklini and D.J. Roth, "Probability of Detection of Internal Voids in Structural Ceramics Using Microfocus Radiography," Journal of Materials Research, vol. 1, number 3, pp. 456-467, 1986. Also NASA TM-87164.

17. L.W. Kessler and D.E. Yuhas, "Acoustic Microscopy - A Tutorial Review," pp. 275-299 in Acoustical Imaging, Vol. 9, Visualization and Characterization, Edited by K.Y. Wang, Plenum, New York, 1980.

18. D.E. Yuhas, and L.W. Kessler "Defect Characterization by Means of the Scanning Laser Acoustic Microsope (SLAM)," pp. 301-313 in Acoustical Imaging, Vol. 9, Visualization and Characterization, Edited by K.Y. Wang, Plenum, New York, 1980.

19. C.H. Chou, B.T. Khuri-Yakub, and G.S. Kino, "Transmission Imaging: Forward Scattering and Scatter Reconstruction, pp. 357-377 in Acoustical Imaging, Vol. 9, Visualization and Characterization, Edited by K.Y. Wang, Plenum, New York, 1980.

20. D. Halliday and R. Resnick, Chapter 38, Fundamentals of Physics, 1974, Revised Printing, Wiley, New York, 1974.

21. D.R. Hull, H.E. Kautz, and A. Vary, "Measurement of Ultrasonic Velocity Using Phase-Slope and Cross-Correlation Methods," Mater. Eval., 43 [11] 1455-1460, (1985).

22. W.T. Cathey, Chapter 2 in Optical Information Processing and Holography, Wiley, New York, 1974.

23. R.P. Bevington, Chapter 4 in Data Reduction and Error Analysis for the Physical Sciences, McGraw-Hill, New York 1969.

1. Report No.	2. Government Accession No.	3. Recipient's Catalog No.
NASA TM-88797		

4. Title and Subtitle	5. Report Date
Quantitative Void Characterization in Structural Ceramics Using Scanning Laser Acoustic Microscopy	6. Performing Organization Code 533-05-01

7. Author(s)	8. Performing Organization Report No.
Don J. Roth, Edward R. Generazio, and George Y. Baaklini	E-3116
	10. Work Unit No.

9. Performing Organization Name and Address	11. Contract or Grant No.
National Aeronautics and Space Administration Lewis Research Center Cleveland, Ohio 44135	
	13. Type of Report and Period Covered Technical Memorandum
12. Sponsoring Agency Name and Address	14. Sponsoring Agency Code
National Aeronautics and Space Administration Washington, D.C. 20546	

15. Supplementary Notes

Prepared for the Basic Science, Electronics, and Glass Divisions Joint Meeting, sponsored by the American Ceramic Society, New Orleans, Louisiana, November 2-5, 1986. Don J. Roth and Edward R. Generazio, NASA Lewis Research Center; George Y. Baaklini, Cleveland State University, Cleveland, Ohio 44115.

16. Abstract

The ability of scanning laser acoustic microscopy (SLAM) to characterize artificially seeded voids in sintered silicon nitride structural ceramic specimens was investigated. Using trigonometric relationships and Airy's diffraction theory, predictions of internal void depth and size were obtained from acoustic diffraction patterns produced by the voids. Agreement was observed between actual and predicted void depths. However, predicted void diameters were generally much greater than actual diameters. Precise diameter predictions are difficult to obtain due to measurement uncertainty and the limitations of 100 MHz SLAM applied to typical ceramic specimens.

17. Key Words (Suggested by Author(s))	18. Distribution Statement
Nondestructive testing; Structural ceramics; Ultrasonics, Ceramics, Silicon nitride; Diffraction; Void/flaw; Acoustic microscopy; Image analysis	Unclassified - unlimited STAR Category 38

19. Security Classif. (of this report)	20. Security Classif. (of this page)	21. No. of pages	22. Price*
Unclassified	Unclassified		

*For sale by the National Technical Information Service, Springfield, Virginia 22161

National Aeronautics and
Space Administration

Lewis Research Center
Cleveland, Ohio 44135

Official Business
Penalty for Private Use $300

SECOND CLASS MAIL

ADDRESS CORRECTION REQUESTED

Postage and Fees Paid
National Aeronautics and
Space Administration
NASA-451

NASA